Naïve Bayesian Precipitation Type Retrieval from Satellite Using a Cloud-Top and Ground-Radar Matched Climatology

HEATHER M. GRAMS

Cooperative Institute for Mesoscale Meteorological Studies, University of Oklahoma, and NOAA/OAR/National Severe Storms Laboratory, Norman, Oklahoma

PIERRE-EMMANUEL KIRSTETTER

Advanced Radar Research Center, University of Oklahoma, Norman, Oklahoma

JONATHAN J. GOURLEY

NOAA/OAR/National Severe Storms Laboratory, Norman, Oklahoma

(Manuscript received 3 March 2016, in final form 5 July 2016)

ABSTRACT

Satellite-based precipitation estimates are a vital resource for hydrologic applications in data-sparse regions of the world, particularly at daily or longer time scales. With the launch of a new generation of high-resolution imagers on geostationary platforms such as the Geostationary Operational Environmental Satellite series R (GOES-R), an opportunity exists to advance the detection and estimation of flash-flood-scale precipitation events from space beyond what is currently available. Because visible and infrared sensors can only observe cloud-top properties, many visible- and infrared-band-based rainfall algorithms attempt to first classify clouds before deriving a rain rate. This study uses a 2-yr database of cloud-top properties from proxy Advanced Baseline Imager radiances from GOES-R matched to surface precipitation types from the Multi-Radar Multi-Sensor (MRMS) system to develop a naïve Bayesian precipitation type classifier for the four major types of precipitation in MRMS: stratiform, convective, tropical, and hail. Evaluation of the naïve Bayesian precipitation type product showed a bias toward classifying convective and stratiform at the expense of tropical and hail. The tropical and hail classes in MRMS are derived based on the vertical structure and magnitude of radar reflectivity, which may not translate to an obvious signal at cloud top for a satellite-based algorithm. However, the satellite-based product correctly classified the hail areas as being convective in nature for the vast majority of missed hail events.

1. Introduction

Real-time estimation of rain and snow rates at hourly and subhourly scales remains a significant challenge in the western United States, where complex terrain limits radar coverage and real-time rain gauge networks are sparse (Maddox et al. 2002). Quantitative precipitation estimation (QPEs) from geostationary satellites offers the advantage of full coverage and spatiotemporal resolution comparable to ground-based radars, particularly with the launch of the Geostationary Operational Environmental Satellite series R (GOES-R) spacecraft. The disadvantage of using spaceborne data from geostationary orbit is the indirectness of the signal (i.e., brightness temperatures radiating from tops of clouds) to precipitation rates experienced at the earth's surface.

The Advanced Baseline Imager (ABI) and Geostationary Lightning Mapper (GLM) instruments aboard GOES-R represent a significant leap forward in terms of geostationary monitoring of clouds and precipitation over the contiguous United States (CONUS; Schmit et al. 2005; Karlson and Smith 2012; Goodman et al. 2013). New spectral bands from the ABI have enabled the development of a suite of cloud-derived products, including cloud-top phase, optical depth, and particle size, and more accurate estimates of cloud-top height and temperature. The cloud-top phase, optical depth,

Corresponding author address: Heather Grams, CIMMS, University of Oklahoma, 120 David L. Boren Blvd., Suite 2100, Norman, OK 73072.
E-mail: heather.moser@noaa.gov

DOI: 10.1175/JHM-D-16-0058.1

© 2016 American Meteorological Society

Brought to you by NOAA Central Library | Unauthenticated | Downloaded 09/22/21 07:18 PM UTC

and particle size will allow for a much improved characterization of cloud-top microphysics than has historically been available from geostationary orbit, which can potentially be useful for classification of precipitation types and QPE over areas that have few other observations.

Many remote sensing rainfall retrieval algorithms perform a basic segregation between convective and stratiform precipitation types, in recognition of the inherent differences between these types in terms of microphysical structure, dynamical processes, and ultimately surface precipitation intensity. Convective/stratiform segregation techniques for active radar systems can involve detection of melting-layer signatures in reflectivity or cross-correlation coefficient for stratiform rain (Awaka et al. 1997; Gourley and Calvert 2003; Brandes and Ikeda 2004), the use of minimum composite reflectivity or vertically integrated liquid thresholds to identify strong convective cores (Zhang et al. 2011; Qi et al. 2013), or analysis of both the horizontal and vertical structure of reflectivity within the storm (Rosenfeld et al. 1995; Steiner et al. 1995; Biggerstaff and Listemaa 2000; Anagnostou 2004).

Precipitation types for spaceborne infrared (IR) rainfall retrievals are necessarily tied to differences in cloud-top properties for convective and stratiform rain. For example, the convective–stratiform technique (CST) assigns areas of influence around local minima in the 10.5–12.6-μm brightness temperature T_b to isolate deep convective cores from the trailing stratiform region in tropical mesoscale convective systems (Adler and Negri 1988). False detections in cirrus shields were removed in CST through the use of a slope parameter derived over a region of neighboring pixels.

More recently, the Precipitation Estimation from Remotely Sensed Information Using Artificial Neural Networks–Cloud Classification System (PERSIANN-CCS) was developed that computed various properties of cloud patch objects such as the minimum and mean temperature, geometric area and shape, temperature gradients, and temperature standard deviations to classify the patches into one of seven clustered groups of patches with similar properties (Hong et al. 2004). No explicit attempt was made to classify cloud patches as convective or stratiform, but the intrinsic differences between height and texture of cloud tops associated with the two precipitation regimes was a motivating factor for the classification scheme for more targeted derivation of T_b–rain-rate curves.

The launch of the 12-channel Spinning Enhanced Visible and Infrared Imager (SEVIRI) on the Meteosat Second Generation (MSG) satellite renewed interest in cloud classification and rainfall estimation in the visible and infrared (VIR) spectral range with the availability of new spectral bands from geostationary orbit well suited to the detection of cloud-top phase, effective particle size, and optical thickness (Kühnlein et al. 2010; Giannakos and Feidas 2013; Kühnlein et al. 2014). These capabilities continue to expand globally with the 2014 launch of the 16-channel Advanced Himawari Imager on the *Himawari-8* spacecraft (Bessho et al. 2016) and the upcoming launch of the 16-channel ABI on GOES-R.

The purpose of this study is to continue efforts to evaluate the value of multispectral derived cloud-top properties for classification of precipitation type from space. The classification will serve as a complement to ground-based products across the CONUS in areas where radar coverage is inadequate, which would then be used to derive satellite-based QPE in order to achieve a seamless, multisensor, high-resolution QPE mosaic nationwide. A new technique is proposed that uses a matched database of ground-radar-derived precipitation types and associated cloud-top properties to drive a naïve Bayesian retrieval of precipitation type probabilities. The naïve Bayesian model not only casts precipitation type classification in a probabilistic form to allow for quantification of uncertainty, but it is also computationally efficient for application to spaceborne sensors that provide information with high temporal frequency (e.g., time scales from 30 s to 15 min). Section 2 will summarize the various data sources used in this study and will provided more details about both the ground-radar-based dataset and the satellite products. Section 3 will describe the naïve Bayesian approach and construction of the cloud product probability distributions. Section 4 provides the results of our analysis in the form of performance metrics, regional distributions, and case studies. Section 5 will summarize the project and provide some general conclusions.

2. Data

The geographic domain for this study was the CONUS as defined for the Multi-Radar Multi-Sensor (MRMS) system, which will be described in more detail in section 2a. The MRMS domain is a rectangular grid that extends from 20° to 55°N latitude and from 130° to 60°W longitude. To derive probability distributions of cloud-top properties for specific precipitation types, a large database was required to ensure that the reference climatology was as close as possible to the full spectrum of rainfall events observed in nature over the study domain. A 2-yr period from 1 January 2011 to 31 December 2012 was selected that represents a nearly complete, uninterrupted record of both 5-min to hourly products from MRMS and 30-min proxy GOES-R cloud-derived

Brought to you by NOAA Central Library | Unauthenticated | Downloaded 09/22/21 07:18 PM UTC

products from *GOES-13* (Greenwald et al. 2016). The only noteworthy period of missing data (aside from rare and sporadic dropouts of the 5-min MRMS products) was a 25-day period from 24 September to 19 October 2012 during which all data from *GOES-13* were unavailable. Entries for the database met the following minimum requirements to be included:

1) MRMS Radar Quality Index (RQI) = 1.0, representing locations where the radar beam is sampling below the melting layer and is unblocked by terrain (Zhang et al. 2012). Requiring a high RQI for the MRMS products ensures that the diagnosed MRMS precipitation type is not degraded because of a lack of observations below the melting layer. Submelting-layer observations are required for the MRMS tropical class, and the hail class's dependence on vertically integrated liquid also requires sufficient vertical coverage.
2) Maximum MRMS radar-based surface precipitation rate $\geq 10\,\text{mm}\,\text{h}^{-1}$ within the GOES-R footprint. The purpose of the rain-rate threshold was to only retain grid points that contained significant precipitation that was likely reaching the surface. One of the limitations of the ground-radar-based QPE is that the height of the radar beam aloft can lead to false detections of light precipitation where it may be evaporating before it reaches the surface (i.e., virga). Furthermore, the focus on flash flood detection in this work motivated the desire to isolate moderate to heavy rain rates over light precipitation.
3) At least 30% of the MRMS grid boxes matched to a GOES-R proxy grid point contain nonzero precipitation rates.
4) No MRMS grid point can be classified as snow within the GOES-R footprint.
5) GOES-R proxy cloud type (described in section 2b) must be one of the six types associated with clouds capable of precipitation: warm rain, supercooled liquid water, thick ice, cirrus, multilayer, or overshooting tops.

a. Radar-derived fields: The MRMS system

The MRMS system integrates approximately 180 operational radars across the CONUS and southern Canada with numerical weather prediction (NWP) analyses of the environment, lightning data, and rain gauge observations to produce seamless reflectivity mosaics along with derived severe weather and QPE products at a high spatiotemporal resolution (0.01° grid spacing and 2-min updates). Zhang et al. (2016) summarized the history of MRMS and all products that are available operationally from the National Centers for Environmental Prediction (NCEP). Three MRMS products were archived for our entire 2011–12 database period: instantaneous surface precipitation rate (SPR), surface precipitation type (SPT), and RQI.

The instantaneous SPR in MRMS is derived directly from the SPT product through use of rain-rate (reflectivity) [i.e., $R(Z)$] relationships assigned to different precipitation type classes. While the precipitation types have expanded in recent years to include two stratiform rain classes (warm and cool season) and a subdivision of the tropical class to delineate stratiform and convective regions (called "tropical stratiform" and "tropical convective"), the 2011–12 archive was produced using an earlier form of the SPT that only had five major classes: stratiform, convective, tropical, hail, and snow (Zhang et al. 2011). For all practical purposes, collapsing the separate stratiform and tropical classes to "stratiform" and "tropical," respectively, in the current MRMS SPT would produce the same precipitation type delineation that would have been available in 2011 and 2012. Convective and hail classes were not changed with the update.

Discrimination between stratiform and convective precipitation types in MRMS is based on minimum thresholds in composite reflectivity, vertically integrated liquid, or reflectivity above the −10°C isotherm, which means that the separation is highly dependent on radar observables. This method works well for single-polarization radar QPE applications because of minimal differences in convective, tropical, and stratiform $R(Z)$ power curves at low reflectivity ranges (e.g., $<30\,\text{dB}Z$); however, using the thresholds in this way leads to precipitation type delineation where only strong convective updraft cores are classified as convective, while all surrounding areas of low reflectivity are classified as stratiform regardless of storm dynamics and morphology.

RQI is a unitless quantity that ranges from 0.0 to 1.0 and was designed to be an indicator of where beam blockage, melting-layer height, and overall radar coverage gaps may limit radar sampling of precipitation for QPE applications (Zhang et al. 2012). Figure 1 shows an example of the RQI product for the CONUS valid at 0000 UTC 28 October 2014. The RQI product reveals lower-quality radar measurements for surface QPE to the northwest of a cold front draped across the central plains. Behind the advancing cold front, there were lower melting-layer heights such that the ranges at which radars can measure liquid phase hydrometeors below the melting layer were limited. There are also significantly lower values of RQI in the Intermountain West of the CONUS because of intervening mountain blockages combined with lower melting-layer heights. In contrast, the warmer air mass in the eastern part of

Brought to you by NOAA Central Library | Unauthenticated | Downloaded 09/22/21 07:18 PM UTC

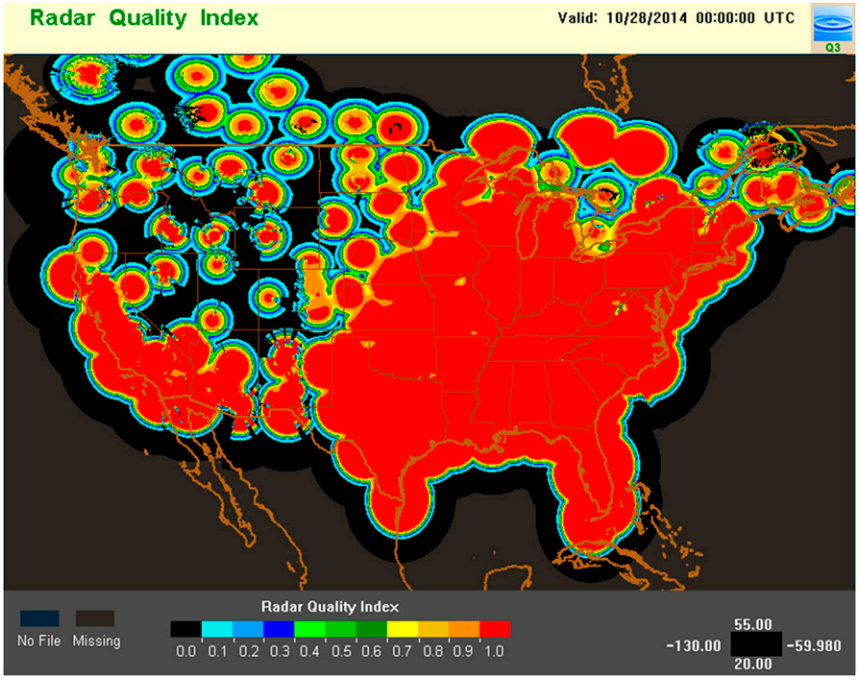

FIG. 1. Example MRMS RQI display for all CONUS WSR-88D radars and Canadian radars at 0000 UTC 28 Oct 2014.

the CONUS allows for radar sampling of liquid precipitation (i.e., RQI = 1.0) at much farther ranges.

b. *Cloud-top properties*

Although GOES-R had not yet launched at the time of this study, proxies of the cloud-derived products were developed by the GOES-R Algorithm Working Group based on a combination of existing channels from GOES-East and GOES-West and simulation of new channels through NWP and radiative transfer model calculations (Greenwald et al. 2016). The purpose of the proxy dataset was to facilitate development of new products and techniques based on the ABI bands such that they would be ready for testing and operational use soon after GOES-R becomes operational. Technical documentation and validation results for all the GOES-R ABI cloud-derived products has been published online by the GOES-R Program (http://www.goes-r.gov), but brief descriptions of several products relevant to this work will also be described here for convenience. The products used for the training database were: cloud type, cloud-top height (converted from MSL to AGL), cloud-top temperature, cloud-top optical depth, and cloud-top effective radius.

Cloud-top phase and type are based on four IR bands from ABI centered on 7.4, 8.5, 11, and 12 μm, respectively. Because no visible channels are included, the cloud-top phase and type are available both day and night. There are six primary cloud types: liquid water, supercooled water, mixed phase, thick ice, thin ice, and multilayered clouds. The cloud phase product has similar categories but collapses all ice-topped clouds to a single ice class (i.e., liquid water, supercooled water, mixed phase, and ice). The phase discrimination is based on the work of Pavolonis (2010), who proposed the use of effective absorption optical depth ratios between two spectral channels, or β ratios, which were more closely related to cloud microphysics and less sensitive to background radiance contamination than traditional techniques based on T_b or spectral T_b differences. An additional advantage of classifying cloud composition in β space is a clear separation between radiances predominantly originating from water or ice clouds and those originating from other sources such as volcanic ash and dust (Pavolonis 2010). A median filter is applied to the β fields prior to classification of cloud types to mitigate speckles and noise. In the GOES-R proxy cloud products evaluated in this study for the years 2011–12, the ''mixed phase'' class was not yet available, while a seventh class for ''overshooting tops'' was included. The six categories included here are thus liquid water (i.e., warm rain), supercooled water, thick ice, cirrus (i.e., thin ice), multilayered clouds, and overshooting tops.

Cloud-top height, temperature, and pressure are based on three IR bands from ABI centered on 11, 12, and 13.3 μm, respectively. As with the cloud phase and

Brought to you by NOAA Central Library | Unauthenticated | Downloaded 09/22/21 07:18 PM UTC

cloud type products, relying solely on IR channels allows the cloud-top height and temperature to be available day and night with no transitional discontinuities. The 11- and 12-μm bands are within spectral windows while the 13.3-μm band experiences strong absorption by carbon dioxide (CO_2) in the atmosphere. The CO_2 absorption is advantageous for monitoring the cloud-top height, especially for optically thin cirrus, because both the background surface and lower atmosphere are totally obscured. The availability of all three of these bands on ABI led to the development of a cloud-top height algorithm by Heidinger et al. (2010) that combined the relative strengths of two preexisting two-channel techniques: split window and CO_2 slicing. Cloud-top temperature is computed first using the hybrid CO_2/split-window method, and then the associated height and pressure are derived by matching the cloud-top temperature to analyzed temperature profiles from an NWP model. Cloud-top temperature is the only product that will be available at the native ABI resolution. Height and pressure will be disseminated with 10-km grid spacing for full disk and CONUS scans and will be updated hourly.

Cloud optical depth and cloud-top particle size use a combination of one visible channel (0.64 μm, or the "red" band) and one near-IR channel (2.25 μm). Because of the dependence on a visible channel, the methodology described here is only applicable when there is sufficient backscattered solar radiation (i.e., during daytime hours). While an IR-based nighttime algorithm for optical depth and particle size has been developed for the ABI, it was not made available for the 2011–12 cloud products proxy dataset; thus, the database compiled for this study was limited to daytime observations. Variations in cloud optical depth can be almost entirely explained using information in the 0.64-μm channel as input to a radiative transfer model if the phase of the cloud particles is known (Walther et al. 2011). After a correction to account for scattering and absorption by the atmosphere, the attenuation of solar radiation can be shown to be proportional to the number of scattering particles along the transmission path, which determines the cloud's optical thickness (Walther and Heidinger 2012). Both optical depth and cloud-top particle size can then be retrieved by using a combination of the visible channel and a near-IR channel.

3. Methodology

a. Overview of naïve Bayesian formulation

Naïve Bayesian classification is a simple but powerful tool for generating probabilities of output classes if the probability distributions of the predictors are known and can be treated as statistically independent. The assumption of statistical independence between the predictor variables is the defining characteristic that distinguishes naïve Bayes classifiers from classic Bayes classifiers. The classic Bayes theorem states that the conditional probability of a particular outcome y given the state vector $\mathbf{x}$ can be derived from

$$P(y\,|\,\mathbf{x}) = \frac{P(y)P(\mathbf{x}\,|\,y)}{P(\mathbf{x})}, \tag{1}$$

where $P(y)$ is the prior probability regardless of $\mathbf{x}$, $P(\mathbf{x}\,|\,y)$ is the posterior probability or the "likelihood" of the $\mathbf{x}$ observations when the outcome y is observed, and $P(\mathbf{x})$ is probability of occurrence for the particular set of features contained in $\mathbf{x}$.

Cast in the context of this study, the outcome y is a particular precipitation type (stratiform, convective, etc.), and the state vector $\mathbf{x}$ is a set of cloud-top observations at a pixel (cloud-top height, temperature, particle size, and optical depth). In classical Bayesian classifiers, there is no assumption of independence among the observations in $\mathbf{x}$ and the conditional joint probabilities must be fully accounted for. For example, for three cloud-top variables, the full expression of the Bayes equation would be

$$P(y\,|\,\mathbf{x}) = \frac{P(y)P(x_1\,|\,y)P(x_2\,|\,y,x_1)P(x_3\,|\,y,x_1,x_2)}{P(x_1)P(x_2\,|\,x_1)P(x_3\,|\,x_1,x_2)}. \tag{2}$$

While this problem may be somewhat tractable for three predictors despite the additional computational overhead, the solution space for the joint probabilities quickly becomes prohibitive when additional predictors are added because of the N^N dimensionality. Adequately capturing the conditional joint probabilities also requires an ever-increasing amount of training data with higher dimensions in order to fully populate the nonparametric probability matrices.

In a naïve Bayes classifier, when the predictors in $\mathbf{x}$ are assumed to be independent, the $P(\mathbf{x}\,|\,y)$ terms collapse to a much more manageable form:

$$P(y\,|\,\mathbf{x}) = \frac{P(y)P(x_1\,|\,y)P(x_2\,|\,y)P(x_3|y)}{P(x_1)P(x_2)P(x_3)}, \tag{3}$$

where each observation in $\mathbf{x}$ can be expressed as a separate probability distribution.

Before proceeding with the naïve Bayesian classification, a quick analysis was conducted to determine the intercorrelation of various cloud-derived products in the GOES-R proxy dataset. Figure 2 shows the range of daily estimates of correlation coefficient for the 2-yr

Brought to you by NOAA Central Library | Unauthenticated | Downloaded 09/22/21 07:18 PM UTC

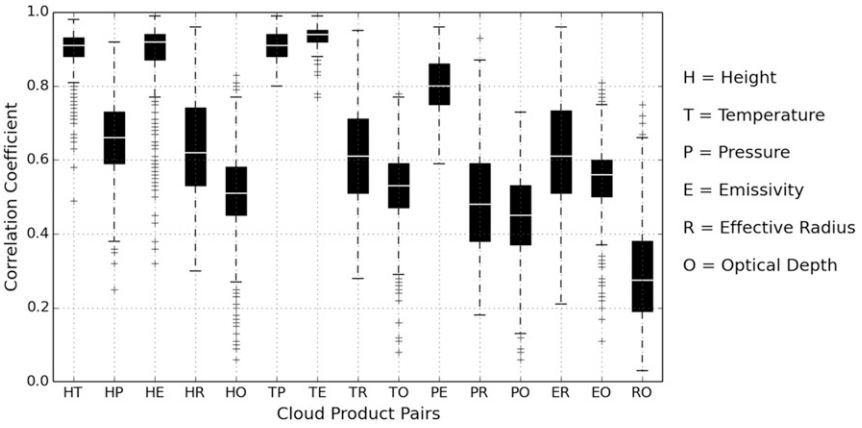

FIG. 2. Distributions of daily correlation coefficient between various GOES-R proxy cloud product pairs during the full 2011–12 database period. White lines in the box plots represent the median value, and boxes represent the interquartile range (25th–75th quartiles). The upper and lower whiskers represent the 95th and 5th percentiles, respectively.

database period. Unsurprisingly, cloud-top height, temperature, and pressure are all highly correlated with each other, along with the 11-μm cloud emissivity. While emissivity was included in the proxy database and can be a useful parameter for detection and monitoring of convection (Cintineo et al. 2013), it was left out of the final Bayesian classifier because it is not planned to be released as part of the initial operational baseline of products from GOES-R. Optical depth and particle size (effective radius) show moderate correlation with other variables and each other, but the correlation appears to be highly variable from day to day with a broad range for the middle 95% of data points. Based on this analysis, we decided to limit our analysis to four cloud products: cloud-top height, cloud-top temperature, cloud-top particle size, and cloud optical depth.

While cloud-top height and temperature were strongly correlated, both of them were kept because both variables tend to have limitations when used on their own. Although cloud-top temperature would be available from GOES-R at a higher spatiotemporal resolution, temperatures of cloud tops have a seasonal and geographic dependence that could impact the classification, particularly between shallow convection and warm versus cool season stratiform clouds. Including cloud height in the joint probability helps to address the seasonal variation and can better segregate stratiform and convective pixels, despite its degraded resolution. It may be necessary to resample the 10-km cloud-top height product to match the geospatial parameters of the other products and recover some of the subgrid variability lost from the aggregation to 10 km.

All entries in the 2011 training database were first segregated by cloud type such that each cloud type would have its own set of cloud-top probability density functions (PDFs) and precipitation type distribution, and hence its own naïve Bayesian classifier. The reasoning for this first breakdown of the database was the expectation that certain cloud types (e.g., overshooting tops) would have vastly different cloud-top properties and precipitation type frequencies than others (e.g., warm rain). This was indeed the case (Fig. 3), but an unanticipated outcome of the cloud type segregation was that all four MRMS precipitation types were still represented for all cloud types, albeit in different proportions. For example, 11% of the pixels matched to the overshooting tops cloud type were deemed to be stratiform according to the MRMS decision-tree logic. Overshooting tops are more indicative of localized updrafts and are therefore expected to be convective precipitation types. It is possible that there were weak updrafts that did not meet the MRMS convective criteria but still resulted in overshooting tops. These types of nuances in the classification schemes can result in some of the algorithmic differences.

The prior probability of each precipitation type, $P(y)$, was computed to be its relative frequency among all four MRMS precipitation types for rain (stratiform, convective, tropical, and hail) based on all database entries from 2011, conditioned on the cloud type. Once the 2011 database was segregated by cloud types, discrete probability distributions were constructed for cloud-top height (converted from MSL to AGL), cloud-top temperature, cloud-top particle size, and optical depth, and these distributions drive the values in the denominator of the naïve Bayesian formula [i.e., $P(x_k)$]. They were stored in text lookup tables for rapid retrieval. For the posterior probability values $P(x_k, y)$, additional probability distributions were stored in lookup tables for each of the four precipitation

Brought to you by NOAA Central Library | Unauthenticated | Downloaded 09/22/21 07:18 PM UTC

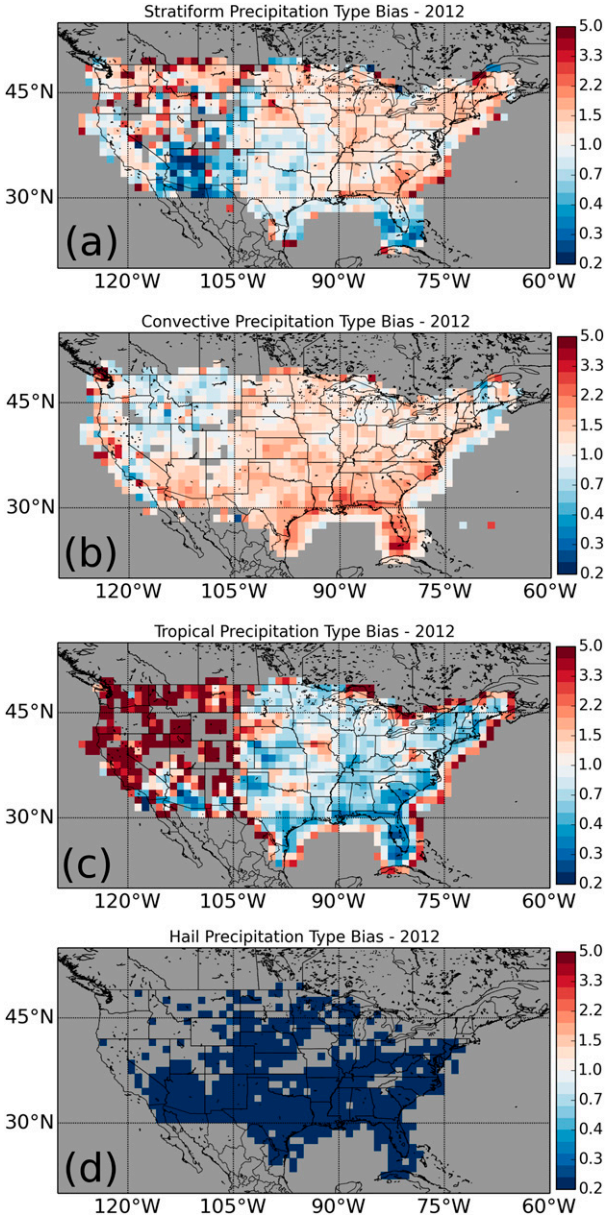

FIG. 3. Bias ratio for the satellite-based precipitation types in 2012 relative to the following MRMS precipitation type classifications: (a) stratiform, (b) convective, (c) tropical, and (d) hail.

types conditional on the cloud type. In other words, 24 separate database queries were made for all entries matching one of six cloud types and one of four precipitation types, and the results of those queries produced the resulting cloud product PDFs. In the final classification algorithm, when a pixel needs to be classified, it retrieves specific lookup tables based on the pixel's cloud type.

The grid spacing difference between the GOES-R proxy data (approximately 4 km) and the MRMS data (0.01°) was such that each GOES gridbox footprint contained anywhere from 15 to 100 MRMS pixels, depending on latitude. Because we were working with discrete precipitation type classes rather than continuous variables, a method had to be established for how to determine the representative MRMS precipitation type for the cluster of grid points matched to a single GOES measurement of cloud-top properties. The nearest-neighbor sample of MRMS pixels matched to the GOES latitude and longitude were collapsed as follows:

1) If any MRMS pixel is classified as hail, the representative class is "hail."
2) If no hail pixels are found, the representative class is "convective" if any MRMS pixels are classified as convective.
3) If no convective or hail pixels are found, the representative class is "tropical" if any MRMS pixels are classified tropical.
4) Finally, if the only precipitation type found is stratiform, the representative class is "stratiform."

b. *Classification of snow*

When constructing the training database, *GOES-13* grid points that overlapped any MRMS points classified as snow were excluded such that the Bayesian algorithm only attempts to classify different types of rain. In the final precipitation type classification algorithm, frozen surface precipitation was diagnosed separately as a function of the surface elevation and the height of the MRMS brightband bottom product. The brightband bottom product is an output of the automated brightband identification algorithm developed by Zhang et al. (2008) and represents the height of the bottom of the melting layer within which brightband enhancement can occur. It is derived by using an NWP analysis of freezing-level height as the first background guess of the brightband top and is adjusted based on the height of brightband signatures observed by the national WSR-88D radar network. The brightband bottom is defined at a height of no more than 700 m below the radar-detected brightband peak. By using the bottom of the bright band rather than the top, the "snow" class therefore includes mixed phase and melting hydrometeors. This classification of snow regions is anticipated to be a temporary approach until more sophisticated winter surface precipitation type classification methods are available (e.g., Elmore 2011; Schuur et al. 2013; Elmore et al. 2014).

4. Results

a. *Statistical verification*

Satellite-based precipitation types were produced for every database entry during the 2012 verification period

Brought to you by NOAA Central Library | Unauthenticated | Downloaded 09/22/21 07:18 PM UTC

TABLE 1. Contingency table verification scores for the naïve Bayesian precipitation type algorithm when compared against the four MRMS precipitation types. Cloud types are defined as All = all types, WR = warm rain, SUP = supercooled liquid water, TI = thick ice, CIR = cirrus (i.e., thin ice), ML = multilayer, and O = overshooting tops. The "count" column represents the number of entries available for that category from the 2012 verification database.

Cloud type	HSS	POD	FAR	HR	CSI	ETS	BIAS	Count
All								
All	0.21	0.41	0.59	0.70	0.26	0.12	1.00	14 157 577
Stratiform								
All	0.24	0.42	0.61	0.74	0.25	0.14	1.08	2 999 813
WR	0.04	0.25	0.60	0.59	0.18	0.02	0.63	146 161
SUP	0.19	0.56	0.63	0.63	0.29	0.10	1.51	373 487
TI	0.25	0.43	0.61	0.75	0.26	0.14	1.13	1 307 050
CIR	0.26	0.52	0.55	0.69	0.32	0.15	1.17	636 288
ML	0.16	0.30	0.67	0.74	0.19	0.09	0.92	348 140
O	0.09	0.09	0.69	0.87	0.07	0.05	0.29	188 687
Convective								
All	0.06	0.63	0.58	0.51	0.34	0.03	1.48	5 587 352
WR	0.01	0.78	0.62	0.44	0.34	0.01	2.08	148 945
SUP	0.07	0.63	0.54	0.52	0.36	0.03	1.37	604 337
TI	0.06	0.55	0.59	0.53	0.30	0.03	1.36	2 473 883
CIR	0.10	0.63	0.56	0.53	0.35	0.05	1.45	923 435
ML	0.04	0.67	0.53	0.51	0.38	0.02	1.42	810 476
O	0.03	0.82	0.60	0.45	0.36	0.01	2.06	626 276
Tropical								
All	0.12	0.26	0.61	0.68	0.19	0.06	0.66	3 924 635
WR	0.00	0.00	0.76	0.89	0.00	0.00	0.00	43 706
SUP	0.01	0.02	0.73	0.82	0.02	0.01	0.06	246 406
TI	0.09	0.33	0.60	0.62	0.22	0.05	0.82	2 162 438
CIR	0.12	0.19	0.62	0.75	0.14	0.07	0.49	520 947
ML	0.09	0.24	0.71	0.72	0.15	0.05	0.80	374 024
O	0.10	0.22	0.52	0.64	0.18	0.05	0.47	577 144
Hail								
All	0.01	0.00	0.67	0.88	0.00	0.00	0.01	1 645 777
WR	0.00	0.00	0.44	0.84	0.00	0.00	0.00	63 484
SUP	0.00	0.00	0.68	0.87	0.00	0.00	0.00	184 241
TI	0.01	0.01	0.64	0.90	0.00	0.00	0.01	671 295
CIR	0.00	0.00	0.78	0.89	0.00	0.00	0.02	256 384
ML	0.00	0.00	0.74	0.86	0.00	0.00	0.00	240 452
O	0.01	0.01	0.61	0.86	0.01	0.01	0.02	229 921

using cloud-top PDFs and MRMS precipitation type distributions derived from the 2011 data. Binary contingency tables were constructed for each of the four primary rain precipitation types (stratiform, convective, tropical, and hail), such that the MRMS type is treated as the target class and any other is treated as a misclassification. From those contingency tables, standard forecast verification metrics were computed: probability of detection (POD), false alarm rate (FAR), hit rate (HR), Heidke skill score (HSS), critical success index (CSI), equitable threat score (ETS), and bias ratio (BIAS) (Wilks 1995). For clarity, the bias ratio represents the ratio of the number of times a class is predicted (e.g., the satellite algorithm) over the number of times the class is observed (MRMS), so BIAS values greater than one represent overprediction of a class. In addition to computing these metrics as aggregate values for all database events, the metrics were also computed for each of the six precipitating cloud types from GOES-R: warm rain, supercooled liquid, thick ice, cirrus, multilayer, and overshooting tops. A summary of all the scores is provided in Table 1.

Based on HSS and ETS, the stratiform and tropical types from satellites tended to most consistently match the collapsed MRMS types. The convective class had lower HSS and ETS but resulted in the highest CSI of the four classes, which may be in part because of its higher frequency of classification (Schaefer 1990). In addition to being the most frequent precipitation type classified, convective also had the highest POD along with a relatively lower FAR. The POD and FAR for the stratiform and tropical classes varied with the cloud type. For example, the cloud types with the highest POD in stratiform rain were supercooled water and cirrus,

Brought to you by NOAA Central Library | Unauthenticated | Downloaded 09/22/21 07:18 PM UTC

while for the tropical rain the highest were thick ice and multilayer clouds. As expected, the satellite-based classification algorithm struggled to ''correctly'' classify the stratiform pixels where overshooting tops were identified, whereas the POD for the convective class associated with overshooting tops was 0.82. The combination of extremely low POD with high HR for the hail class is indicative of both the underprediction of hail where it is observed in MRMS and the presence of a large number of ''correct null'' events given that hail was the rarest class of the four. Further analysis of the satellite algorithm's treatment of hail is provided later in this section.

In terms of relative bias in Table 1, broadly speaking, the convective and stratiform classes tended to be used more often in the satellite algorithm than they were observed in MRMS at the expense of the tropical and hail classes. The differences were a bit more nuanced when the database was subdivided by cloud type. Despite overall having a slightly high bias for 2012, the bias for the stratiform class was dominated by overprediction in the three most common cloud types (thick ice, cirrus, and supercooled water). The bias is less than one where warm rain, multilayer clouds, and overshooting tops were identified. The warm rain and overshooting tops types were predominantly classified as convective. While the tropical class was underpredicted overall, the bias is highly variable by cloud type, with thick ice and multilayer clouds showing the most consistency to MRMS. By contrast, the warm rain and supercooled water types were almost never classified as tropical, which may be because of the shallow nature of these cloud types and low reflectivity of the precipitation.

Also included in Table 1 is a breakdown of raw event counts contained in each precipitation type and cloud type. Events are defined as a single, instantaneous GOES-R proxy grid point that is matched to the relevant MRMS products and meets the selection criteria defined in section 2. Of the approximately 14 million database events from 2012, 39.5% were classified as convective using the collapsed MRMS precipitation type classification, 27.7% were tropical, 21.2% were stratiform, and 11.6% were hail. A large majority of the GOES-R proxy cloud types observed were classified as thick ice (46.7%), followed distantly by cirrus (16.5%). In the GOES-R ''cloud phase'' product, which is the initial baseline operational cloud type that will be available, the thick ice and cirrus types will be combined as a single ''ice'' class, which will therefore comprise over 60% of all cloud types.

b. *Geographical analysis*

Figure 3 illustrates how the bias ratio varies by region over the CONUS for each of the four precipitation types

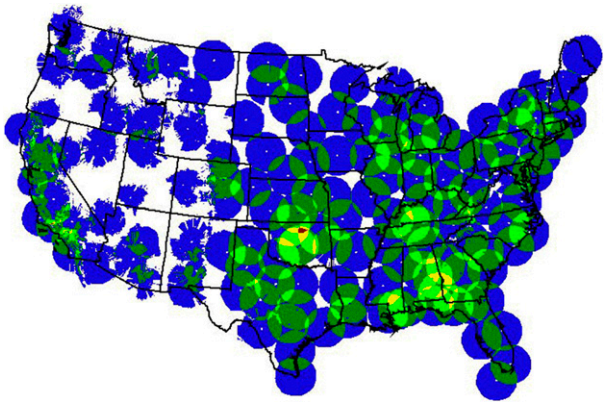

FIG. 4. Coverage of the WSR-88D radar network over the CONUS at or below 3 km AGL (Maddox et al. 2002).

in 2012. The database events were binned into 1.0° latitude–longitude grid boxes over the MRMS domain. Bias values greater (less) than one indicate that the naïve Bayesian model produces more (less) of that precipitation type than MRMS. Broadly speaking, the gaps and variability characteristic of the western half of the United States were a result of poor ground-radar coverage and low sample sizes of ''good quality'' observations in MRMS, as defined by the RQI and minimum rain-rate criteria for inclusion in the database. Over the relatively well-sampled eastern half of the CONUS, the satellite precipitation type tends to favor stratiform and convective, with tropical and hail less likely to be classified than they would be in MRMS.

The geographical distribution of the tropical precipitation type bias strongly correlated with the quality and density of ground-radar coverage (Fig. 4), which is an artifact of the MRMS product used in the comparison rather than a reflection of any tendency in the satellite-based algorithm. One of the criteria for tropical classification in MRMS is the detection of a ''low-echo centroid'' feature in the vertical profile of reflectivity (VPR) that is indicative of efficient warm rain processes (Xu et al. 2008). Therefore, the MRMS tropical class is critically dependent on the availability of sufficient radar measurements below the melting layer for a vertical reflectivity gradient to be computed. If observations below the melting layer were limited or unavailable, the tropical class was not invoked. While the bias ratio distribution in Fig. 3 would imply that the naïve Bayesian algorithm was underpredicting the tropical class relative to MRMS in areas of good low-level radar coverage, the MRMS SPT has a well-documented tendency to classify rain as tropical too often, particularly in the warm season (Chen et al. 2013). It is possible that the cloud-top properties associated with the MRMS tropical class are not sufficiently different from the stratiform or

Brought to you by NOAA Central Library | Unauthenticated | Downloaded 09/22/21 07:18 PM UTC

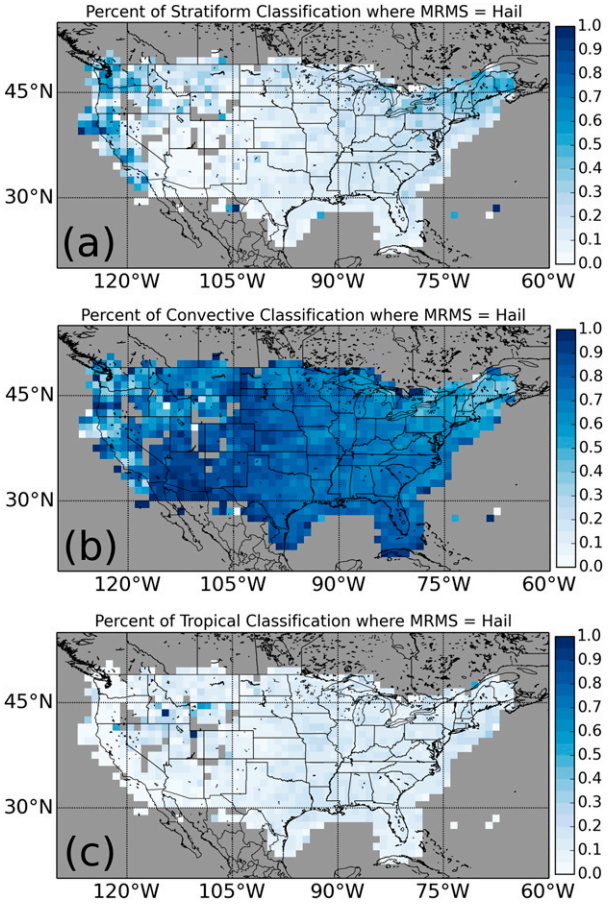

FIG. 5. Percent of events classified as (a) stratiform, (b) convective, and (c) tropical where the MRMS precipitation type was classified as hail.

convective cloud-top properties because many of the tropical pixels are in fact misclassified in MRMS. Additionally, the definition of the tropical precipitation type in MRMS as being based on vertical reflectivity structure near the ground suggests that correctly identifying it from cloud-top information alone would be challenging.

To further investigate the cause of the significant underprediction of the hail category by the satellite-based algorithm, we evaluated the naïve Bayesian probabilities of the three nonhail classes for locations that were classified as hail by MRMS (Fig. 5). With some possible exceptions over New England and the U.S. West Coast, the dominant alternative classification to hail was convective. In MRMS, the hail category is defined as an extension to convective that is only invoked based on a minimum threshold of the radar-derived maximum expected size of hail (MESH) product in order to apply an upper limit on convective rain rates where hail contamination is likely (Zhang et al. 2016). Therefore, it is not surprising that from the point of view of a spaceborne sensor, there was no discernable difference between cloud tops classified as convective and those classified as hail. The areas with relatively higher likelihood of stratiform classification tend to correspond with regions where hail and severe hail were rare based on multiyear climatological assessments (Cintineo et al. 2012), which could suggest that vigorous deep convection is also relatively less common. Furthermore, satellite-based rainfall estimation does not have the same sensitivity to the presence of hail as radar-based measurements, so the identification of hail may not be as critical from a QPE accuracy perspective.

c. *Case studies*

To illustrate how the satellite-based precipitation types compare to MRMS for individual rainfall events, snapshots from three different cases and regions are provided here. The first example at 2015 UTC 19 May 2011 shows two different events over the central United States: a broad area of upslope-driven stratiform rain and elevated convection over the northern plains and isolated severe convection over western Oklahoma (Fig. 6). Ground-radar coverage from the WSR-88D network is severely limited over southeastern Montana and eastern Wyoming (Fig. 6c), resulting in large gaps in the MRMS products. The relatively low freezing-level heights during this event resulted in large areas being classified as being within or above the melting layer, which was characterized in the MRMS SPT as the yellow brightband class, which is used only in areas already classified as stratiform precipitation to indicate that the radar beam is sampling mixed phase or ice hydrometeors. Recognizing that bright band is an extension of the stratiform class, there was good agreement between the satellite-based precipitation types of stratiform precipitation (Fig. 6b) with MRMS (Fig. 6a). The spatial consistency with the satellite-based product highlights the potential for filling in QPE gaps in the ground-radar network.

Farther east in areas of the Dakotas and Oklahoma that are well covered by radars, the primary difference between MRMS and the naïve Bayesian classification was the tendency for the satellite-based product to more broadly apply the convective precipitation type. The convective region in South Dakota was associated with a broad area that was classified as overshooting tops in the cloud type product, which could be a misclassification of the cloud type. Because the GOES-R overshooting tops product was under development and is not slated to be included in the baseline suite of operational products, its performance will not be evaluated here. The convective

Brought to you by NOAA Central Library | Unauthenticated | Downloaded 09/22/21 07:18 PM UTC

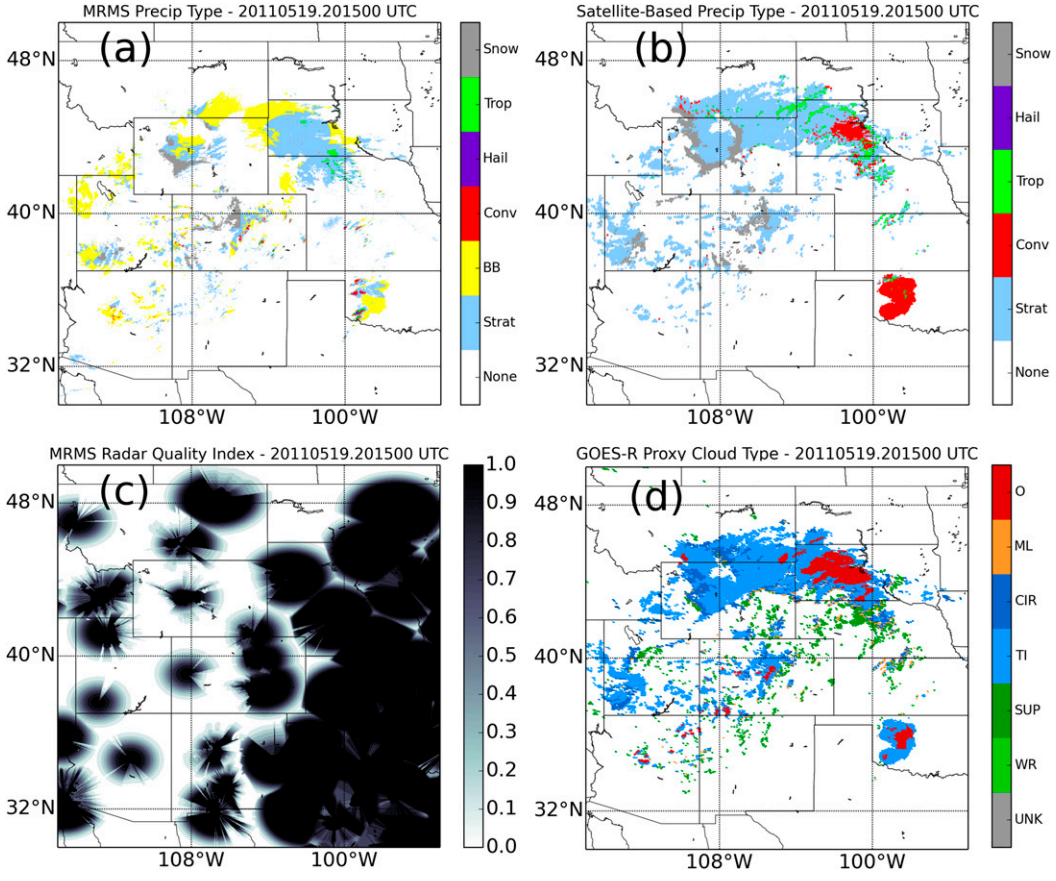

FIG. 6. Comparison of (a) MRMS precipitation type, (b) naïve Bayesian classification of precipitation type from GOES-R proxy cloud properties, (c) MRMS RQI, and (d) GOES-R proxy cloud type valid at 2015 UTC 19 May 2011.

region in Oklahoma was associated with a line of discrete supercells initiating along the dryline. While the MRMS SPT only assigns convective and hail classes to the strongest cores of the storms and applies stratiform and brightband classes to the anvil regions, the satellite-based product broadly classified the storm updrafts and anvils both as convective. The naïve Bayesian algorithm consistently classified convection in this manner for a variety of storm modes, including mesoscale convective systems.

To demonstrate the probabilistic nature of the naïve Bayesian classification, Fig. 7 shows the individual probabilities of each precipitation type for the same event as in Fig. 6. While there were areas where one of the precipitation type probabilities far exceeded those of the other types (e.g., stratiform in central Wyoming), there were other regions where two precipitation types had relatively high probabilities (e.g., the isolated showers in the Four Corners region). A weak local maximum in the hail probabilities existed over southwestern Oklahoma (Fig. 7, bottom right) that corresponded well to the area where hail is classified by MRMS (Fig. 6a) despite the overall low hail probabilities across the area. The final classification in the precipitation type scheme is based on the selection of the precipitation type with the maximum probability at any given location (Fig. 6b), but it may be possible to leverage the individual probabilities in a more seamless fashion that is not dependent on a deterministic classification for each grid point.

The second example case is a synoptic-scale Pacific frontal system over the northwestern CONUS at 2015 UTC 18 January 2012 with rain primarily observed along the West Coast and snow observed across the mountainous areas (Fig. 8). Subjective evaluation of the simple snow classification method employed for the satellite product shows an effective delineation of snow from rain with some subtle differences in transitional zones. The naïve Bayesian classification produced more convective and tropical areas than were identified in MRMS. The naïve Bayesian

Brought to you by NOAA Central Library | Unauthenticated | Downloaded 09/22/21 07:18 PM UTC

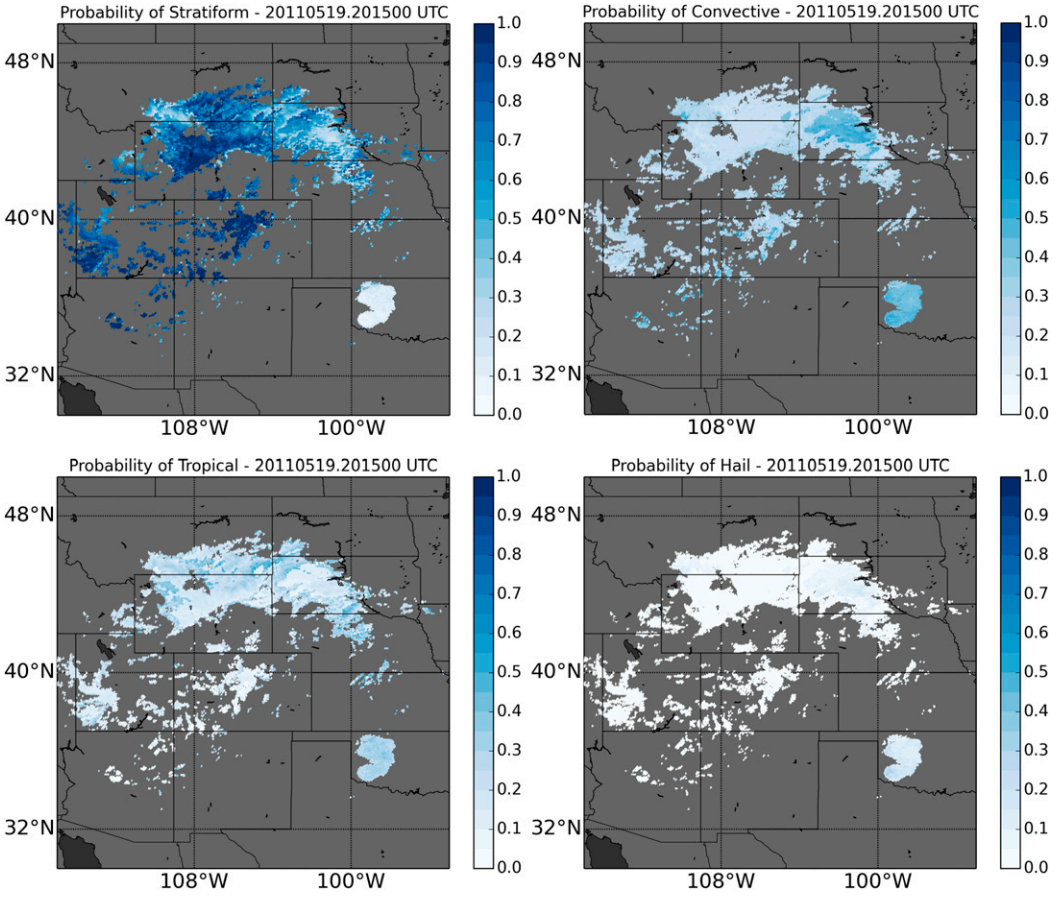

FIG. 7. Individual precipitation type probabilities valid at 2015 UTC 19 May 2011.

classifications also showed greater coverage of precipitation over the region owing to the fact that MRMS is limited by the sparse radar coverage. This again highlights the benefit of satellite-based precipitation type estimates over these regions of poor low-level sampling by ground radars.

The third case example presented was Hurricane Sandy along the eastern coast of the United States (Fig. 9). Hurricane Sandy was a category 1 hurricane centered off the North Carolina coast at 1815 UTC 28 October 2012, where the eye structure is apparent in the GOES-R proxy-based images (Figs. 9b,d). Aside from a lack of ground-based observations over the open ocean, the primary difference between MRMS and the satellite-based algorithm was the use of the tropical precipitation type. Although it has been noted in previous studies (e.g., Chen et al. 2013) that the tropical class is too often invoked in MRMS, for this particular event that was not the case. One reason for the nonuse of the tropical class in MRMS was that much of the low-level reflectivity associated with Sandy was below the 30-dBZ minimum threshold required for MRMS to use the tropical $R(Z)$ relationship for rain rates; thus, the classification of stratiform was used by default. It is also possible that the VPR low-echo centroid criterion was not met for the coastal radars to be classified as tropical, particularly as Hurricane Sandy developed extratropical characteristics as it approached land. Instances such as this case highlight the discrepancies between MRMS and the satellite-based algorithm that may not be deemed as either correct or incorrect. Despite having a more direct measurement using active remote sensing, the MRMS algorithms rely on decision-tree logic that is sensitive to specific thresholds whereas the satellite-based algorithm uses the full PDF.

d. Impact of rain-rate thresholds

As noted in section 2, one of the criteria for inclusion of an observation in the training database was that the maximum MRMS rain rate within a GOES-R gridpoint area must exceed 10 mm h^{-1}. If the maximum rain-rate criteria are met, then all other MRMS grid points within that GOES-R footprint are also included in the

Brought to you by NOAA Central Library | Unauthenticated | Downloaded 09/22/21 07:18 PM UTC

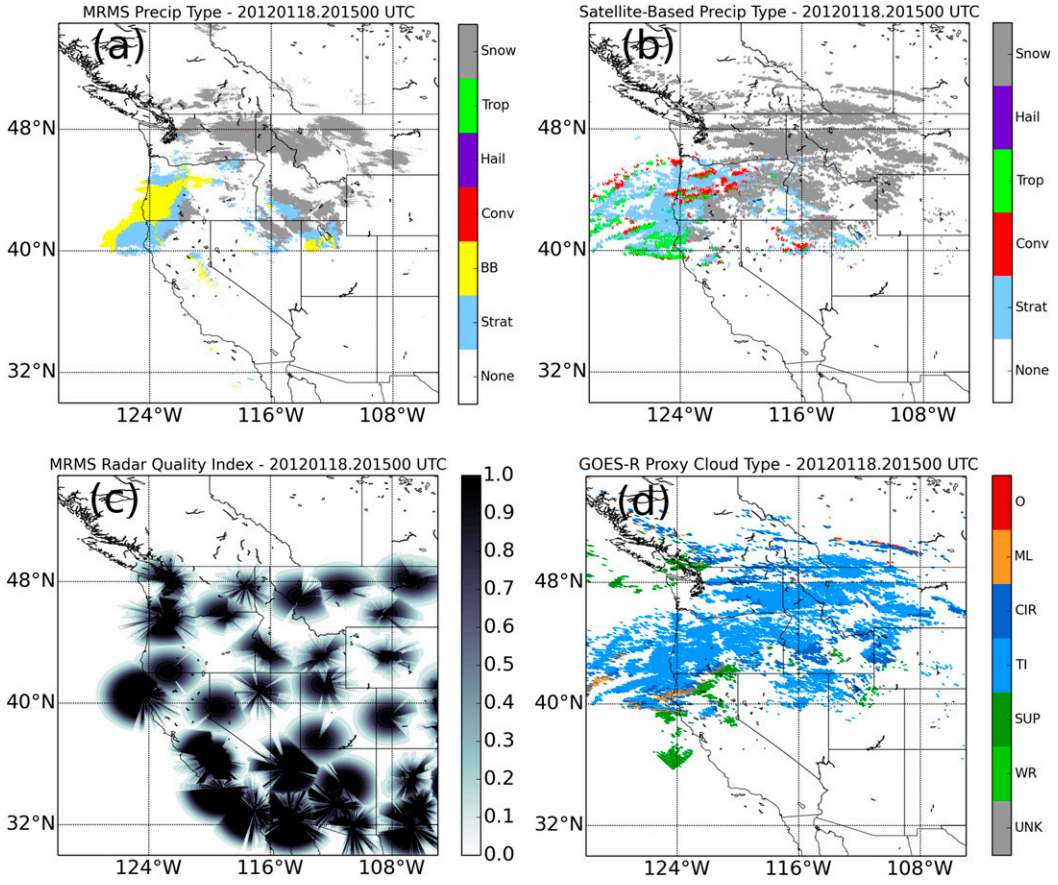

FIG. 8. As in Fig. 6, but for results at 2015 UTC 18 Jan 2012.

database. To assess the impact of that threshold on the resulting precipitation type classification, a second version of the database was constructed using a maximum MRMS rain rate of at least 2.54 mm h^{-1} (0.10 in. h^{-1}). Table 2 contains a similar summary of verification statistics to Table 1 for the lower rain-rate-derived database.

Applying a lower threshold increased the size of the database from 14 million to over 42 million entries. In other words, the GOES-R grid points with higher maximum surface rain rates would only comprise one-third of the samples such that the probability distributions are dominated by observations with lighter precipitation. As a result, the convection-dominant character of the previous model is replaced by a dominance of stratiform precipitation, which is more consistent with the relative frequencies observed in MRMS. The higher likelihood of stratiform classification appears to improve several of the verification metrics over the previous database for stratiform rain in particular, but it seems to have adverse effects on other classes, especially the tropical class.

The tropical classification is not invoked in MRMS unless the lowest elevation reflectivity exceeds 30 dBZ, which is equivalent to a minimum rain rate of at least 3.2 mm h^{-1}. By default, areas with lower reflectivity and a positive tropical identification are classified as stratiform instead. Because the new database is so heavily dominated by lighter precipitation, we feel that this is the reason that the tropical class is far less frequently used. Thus, while the use of a lower rain-rate threshold may more closely represent probability distributions of rainfall observed in nature, it has some deleterious impacts on the classification of precipitation type because of the way the training classes are derived. An intermediate threshold between 2.54 and 10 mm h^{-1} may represent an optimum level such that the stratiform and convective classes are unbiased and the tropical classifications are still represented.

5. Summary and conclusions

A technique for classifying precipitation type from GOES-R cloud-derived products was proposed and

Brought to you by NOAA Central Library | Unauthenticated | Downloaded 09/22/21 07:18 PM UTC

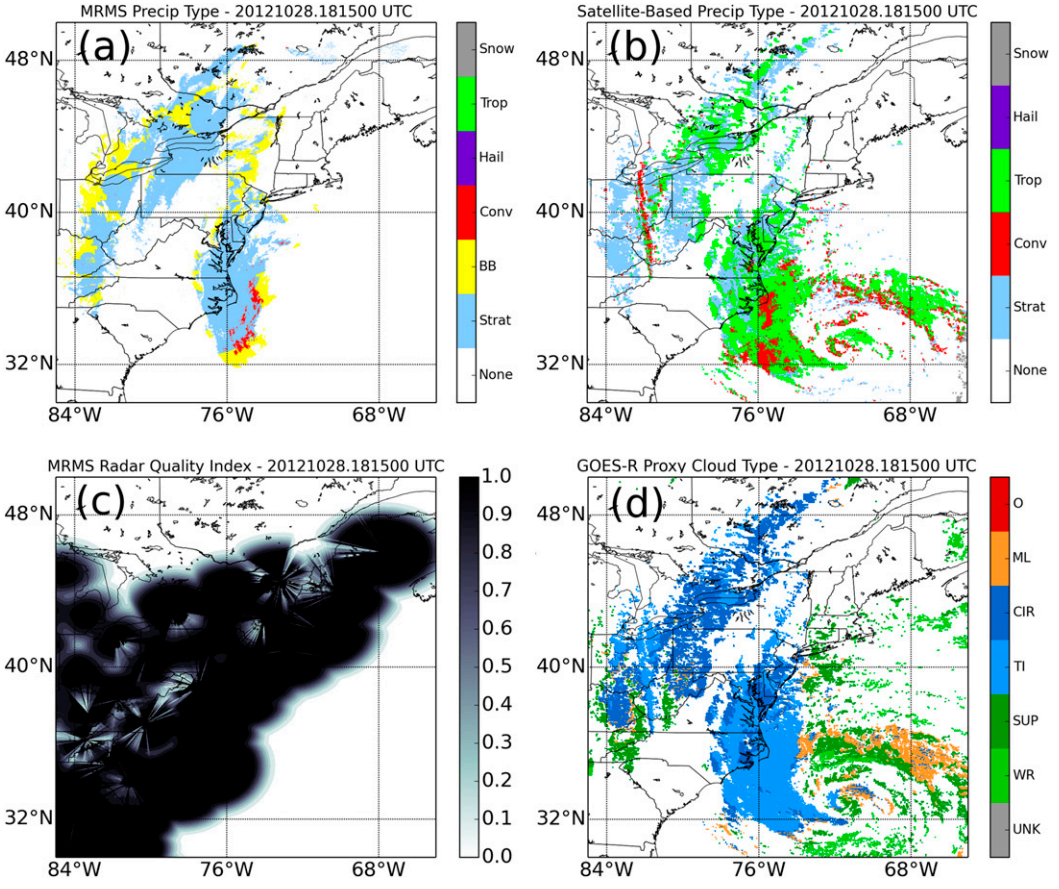

FIG. 9. As in Fig. 6, but for results at 1815 UTC 28 Oct 2012.

evaluated here for the purposes of developing a precipitation-type-driven quantitative precipitation estimate in data-sparse regions of the United States. The precipitation type classification is based on the assumption that stratiform and convective echoes have statistically distinct cloud-top characteristics that can be segregated and classified using a data-driven probabilistic model. PDFs of cloud-top height, temperature, particle size, and optical depth were constructed for different categories of cloud type and MRMS surface precipitation type using a 2-yr database of GOES-R proxy cloud-top products matched to MRMS ground-radar-derived products, and the relative frequency of occurrence of each MRMS precipitation type was also computed. Snow areas were classified using MRMS products that identify the height and depth of the melting layer across the CONUS.

Although the precipitation types produced from the naïve Bayesian model were trained using the MRMS precipitation types as ''truth,'' the resulting classifications showed some differences. Because the tropical and hail classes from MRMS are derived solely from radar-observed criteria, the naïve Bayesian model could not effectively distinguish the cloud-top characteristics of those classes from other areas classified as stratiform or convective. The different behavior of the cloud-top-based classification appeared to make sense physically, however, when evaluating more closely how the precipitation types are applied. Even if the satellite-based algorithm cannot separate hail from convective, it still correctly identified the hail cores as convective as opposed to stratiform or tropical. It also appeared to correctly identify the tropical class in coastal maritime systems even when MRMS does not.

The naïve Bayesian classification generally tends to be biased toward the convective precipitation type, which appears to be associated with the rain-rate threshold chosen for the initial database. A second database constructed using a lower rain-rate threshold (2.54 instead of 10 mm h^{-1}) showed a dominance of stratiform classification instead of convective. Because the precipitation classification methodology in MRMS uses stratiform as the default class where

Brought to you by NOAA Central Library | Unauthenticated | Downloaded 09/22/21 07:18 PM UTC

TABLE 2. As in Table 1, but for contingency table statistics for a training database derived using a max MRMS rain rate of 2.54 mm h^{-1}.

Cloud type	HSS	POD	FAR	HR	CSI	ETS	BIAS	Count
All								
All	0.40	0.55	0.45	0.77	0.38	0.25	1.00	42 329 665
Stratiform								
All	0.17	0.89	0.40	0.61	0.56	0.09	1.50	23 161 621
WR	0.04	0.96	0.37	0.63	0.62	0.02	1.52	808 246
SUP	0.12	0.95	0.34	0.66	0.64	0.07	1.44	3 534 668
TI	0.15	0.89	0.44	0.58	0.53	0.08	1.59	9 460 596
CIR	0.17	0.91	0.33	0.66	0.63	0.09	1.36	5 531 065
ML	0.13	0.86	0.43	0.58	0.52	0.07	1.51	2 813 581
O	0.15	0.63	0.60	0.57	0.32	0.08	1.57	1 013 465
Convective								
All	0.10	0.25	0.67	0.71	0.16	0.05	0.74	9 980 404
WR	0.03	0.06	0.66	0.74	0.06	0.02	0.19	314 776
SUP	0.09	0.14	0.61	0.75	0.11	0.05	0.35	1 284 313
TI	0.09	0.23	0.69	0.71	0.15	0.05	0.76	2 473 883
CIR	0.15	0.25	0.64	0.75	0.17	0.08	0.68	1 820 228
ML	0.10	0.27	0.63	0.67	0.19	0.05	0.72	1 483 221
O	0.00	0.47	0.69	0.51	0.23	0.00	1.53	955 879
Tropical								
All	0.00	0.00	0.57	0.82	0.00	0.00	0.01	7 517 414
WR	0.00	0.00	—	0.92	0.00	0.00	0.00	102 909
SUP	0.00	0.00	—	0.90	0.00	0.00	0.00	567 984
TI	0.01	0.01	0.59	0.78	0.01	0.00	0.01	4 007 597
CIR	0.00	0.00	0.63	0.87	0.00	0.00	0.00	1 151 921
ML	0.00	0.00	—	0.85	0.00	0.00	0.00	793 652
O	0.01	0.01	0.53	0.71	0.01	0.00	0.02	893 351
Hail								
All	0.02	0.01	0.77	0.96	0.01	0.01	0.04	1 670 226
WR	0.00	0.00	0.93	0.95	0.00	0.00	0.00	65 702
SUP	0.02	0.02	0.83	0.96	0.02	0.01	0.10	187 748
TI	0.02	0.01	0.77	0.96	0.01	0.01	0.05	679 544
CIR	0.00	0.00	0.92	0.97	0.00	0.00	0.00	260 692
ML	0.00	0.00	0.83	0.95	0.00	0.00	0.00	244 283
O	0.03	0.02	0.73	0.92	0.02	0.02	0.09	232 257

reflectivity thresholds are not met for the other three classes, selection of a very low rain-rate threshold may place too much weight on stratiform at the expense of the other classes, which was evident in Table 2. For the final version of the algorithm used for QPE, an intermediate threshold between 2.54 and 10 mm h^{-1} should be chosen that achieves unbiased stratiform and convective classification frequency while still allowing for tropical classification. Future work will focus on identifying the appropriate threshold value, which will be need to be completed prior to operational implementation of this algorithm. We will also test alternate methods of defining the MRMS classification to see if requiring more areal coverage of the convective class within the GOES-R grid box reduces the convective overclassification.

A natural next step to this study will be the integration of total lightning observations for a more definitive identification of convection using products that will be readily available from the GLM aboard GOES-R. Because the Cloud Type product from GOES-R is slated as a ''future'' capability and will not be part of the initial baseline, this same technique will be used to derive a precipitation type algorithm that uses the Cloud Phase product, which is similar to Cloud Type but with the ice phase types collapsed into a single ice class. The naïve Bayesian precipitation type model produced from the Cloud Phase classes will be the initial version used in real-time for satellite-derived MRMS QPE products until the Cloud Type product is disseminated from GOES-R operationally. The precipitation type product based on the technique described in this paper, with some future adjustments, will serve as guidance for a precipitation-type-dependent rain-rate algorithm derived from GOES-R. The satellite-based rain rates can potentially serve as a compliment to the MRMS ground-based radar QPE in a gap-filling capacity where radar coverage is either poor or nonexistent.

Brought to you by NOAA Central Library | Unauthenticated | Downloaded 09/22/21 07:18 PM UTC

Acknowledgments. Funding for this project was provided by the GOES-R Program and NOAA/Office of Oceanic and Atmospheric Research under NOAA–University of Oklahoma Cooperative Agreement NA11OAR4320072, U.S. Department of Commerce, which the authors gratefully acknowledge. We also thank Robert Rabin and the three anonymous reviewers for their technical assistance and thoughtful feedback on our analysis and manuscript.

REFERENCES

Adler, R. F., and A. J. Negri, 1988: A satellite infrared technique to estimate tropical convective and stratiform rainfall. *J. Appl. Meteor.*, **27**, 30–51, doi:10.1175/1520-0450(1988)027<0030:ASITTE>2.0.CO;2.

Anagnostou, E. N., 2004: A convective/stratiform precipitation classification algorithm for volume scanning weather radar observations. *Meteor. Appl.*, **11**, 291–300, doi:10.1017/S1350482704001409.

Awaka, J., T. Iguchi, H. Kumagai, and K. Okamoto, 1997: Rain type classification algorithm for TRMM Precipitation Radar. *Proc. 1997 IEEE Int. Geoscience and Remote Sensing Conf.*, Singapore, IEEE, 1633–1635, doi:10.1109/IGARSS.1997.608993

Bessho, K., and Coauthors, 2016: An introduction to Himawari-8/9—Japan's new-generation geostationary meteorological satellites. *J. Meteor. Soc. Japan*, **94**, 151–183, doi:10.2151/jmsj.2016-009.

Biggerstaff, M. I., and S. A. Listemaa, 2000: An improved scheme for convective/stratiform echo classification using radar reflectivity. *J. Appl. Meteor.*, **39**, 2129–2150, doi:10.1175/1520-0450(2001)040<2129:AISFCS>2.0.CO;2.

Brandes, E. A., and K. Ikeda, 2004: Freezing-level estimation with polarimetric radar. *J. Appl. Meteor.*, **43**, 1541–1553, doi:10.1175/JAM2155.1.

Chen, S., and Coauthors, 2013: Evaluation and uncertainty estimation of NOAA/NSSL next-generation National Mosaic Quantitative Precipitation Estimation product (Q2) over the continental United States. *J. Hydrometeor.*, **14**, 1308–1322, doi:10.1175/JHM-D-12-0150.1.

Cintineo, J. L., T. M. Smith, V. Lakshmanan, H. E. Brooks, and K. L. Ortega, 2012: An objective high-resolution hail climatology of the contiguous United States. *Wea. Forecasting*, **27**, 1235–1248, doi:10.1175/WAF-D-11-00151.1.

——, M. J. Pavolonis, J. M. Sieglaff, and A. K. Heidinger, 2013: Evolution of severe and nonsevere convection inferred from GOES-derived cloud properties. *J. Appl. Meteor. Climatol.*, **52**, 2009–2023, doi:10.1175/JAMC-D-12-0330.1.

Elmore, K. L., 2011: The NSSL hydrometeor classification algorithm in winter surface precipitation: Evaluation and future development. *Wea. Forecasting*, **26**, 756–765, doi:10.1175/WAF-D-10-05011.1.

——, Z. L. Flamig, V. Lakshmanan, B. T. Kaney, V. Farmer, H. D. Reeves, and L. P. Rothfusz, 2014: MPING: Crowd-sourcing weather reports for research. *Bull. Amer. Meteor. Soc.*, **95**, 1335–1342, doi:10.1175/BAMS-D-13-00014.1.

Giannakos, A., and H. Feidas, 2013: Classification of convective and stratiform rain based on the spectral and textural features of Meteosat Second Generation infrared data. *Theor. Appl. Climatol.*, **113**, 495–510, doi:10.1007/s00704-012-0802-z.

Goodman, S. J., and Coauthors, 2013: The GOES-R Geostationary Lightning Mapper (GLM). *Atmos. Res.*, **125–126**, 34–49, doi:10.1016/j.atmosres.2013.01.006.

Gourley, J. J., and C. M. Calvert, 2003: Automated detection of the bright band using WSR-88D data. *Wea. Forecasting*, **18**, 585–599, doi:10.1175/1520-0434(2003)018<0585:ADOTBB>2.0.CO;2.

Greenwald, T. J., and Coauthors, 2016: Real-time simulation of the GOES-R ABI for user readiness and product evaluation. *Bull. Amer. Meteor. Soc.*, **97**, 245–261, doi:10.1175/BAMS-D-14-00007.1.

Heidinger, A. K., M. J. Pavolonis, R. E. Holz, B. A. Baum, and S. Berthier, 2010: Using *CALIPSO* to explore the sensitivity to cirrus height in the infrared observations from NPOESS/VIIRS and GOES-R/ABI. *J. Geophys. Res.*, **115**, D00H20, doi:10.1029/2009JD012152.

Hong, Y., K.-L. Hsu, S. Sorooshian, and X. Gao, 2004: Precipitation Estimation from Remotely Sensed Imagery Using an Artificial Neural Network Cloud Classification System. *J. Appl. Meteor.*, **43**, 1834–1852, doi:10.1175/JAM2173.1.

Karlson, D., and M. Smith, 2012: The GOES-R Series: The nation's next-generation geostationary operational environmental satellites. *Earth Sci.*, **28**, 18–24.

Kühnlein, M., B. Thies, T. Naub, and J. Bendix, 2010: Rainfall-rate assignment using MSG SEVIRI data—A promising approach to spaceborne rainfall-rate retrieval for midlatitudes. *J. Appl. Meteor. Climatol.*, **49**, 1477–1495, doi:10.1175/2010JAMC2284.1.

——, T. Appelhans, B. Thies, and T. Nauss, 2014: Improving the accuracy of rainfall rates from optical satellite sensors with machine learning—A random forests–based approach applied to MSG SEVIRI. *Remote Sens. Environ.*, **141**, 129–143, doi:10.1016/j.rse.2013.10.026.

Maddox, R. A., J. Zhang, J. J. Gourley, and K. W. Howard, 2002: Weather radar coverage over the contiguous United States. *Wea. Forecasting*, **17**, 927–934, doi:10.1175/1520-0434(2002)017<0927:WRCOTC>2.0.CO;2.

Pavolonis, M. J., 2010: Advances in extracting cloud composition information from spaceborne infrared radiances—A robust alternative to brightness temperatures. Part I: Theory. *J. Appl. Meteor. Climatol.*, **49**, 1992–2012, doi:10.1175/2010JAMC2433.1.

Qi, Y., J. Zhang, and P. Zhang, 2013: A real-time automated convective and stratiform precipitation segregation algorithm in native radar coordinates. *Quart. J. Roy. Meteor. Soc.*, **139**, 2233–2240, doi:10.1002/qj.2095.

Rosenfeld, D., E. Amitai, and D. B. Wolff, 1995: Classification of rain regimes by the three-dimensional properties of reflectivity fields. *J. Appl. Meteor.*, **34**, 198–211, doi:10.1175/1520-0450(1995)034<0198:CORRBT>2.0.CO;2.

Schaefer, J. T., 1990: The critical success index as an indicator of warning skill. *Wea. Forecasting*, **5**, 570–575, doi:10.1175/1520-0434(1990)005<0570:TCSIAA>2.0.CO;2.

Schmit, T. J., M. W. Gunshor, W. P. Menzel, J. J. Gurka, J. Li, and A. S. Bachmeier, 2005: Introducing the next-generation Advanced Baseline Imager on GOES-R. *Bull. Amer. Meteor. Soc.*, **86**, 1079–1096, doi:10.1175/BAMS-86-8-1079.

Schuur, T. J., A. V. Ryzhkov, H. D. Reeves, J. Krause, M. R. Kumjian, K. L. Elmore, and K. L. Ortega, 2013: A new surface-based polarimetric hydrometeor classification algorithm for the WSR-88D network. *36th Conf. on Radar Meteorology*, Breckenridge, CO, Amer. Meteor. Soc., 7B.3. [Available online at https://ams.confex.com/ams/36Radar/webprogram/Paper228523.html.]

Steiner, M., R. A. Houze, and S. E. Yuter, 1995: Climatological characteristics of three-dimensional storm structure from operational radar and rain gauge data. *J. Appl. Meteor.*, **34**, 1978–2007, doi:10.1175/1520-0450(1995)034<1978:CCOTDS>2.0.CO;2.

Brought to you by NOAA Central Library | Unauthenticated | Downloaded 09/22/21 07:18 PM UTC

Walther, A., and A. K. Heidinger, 2012: Implementation of the Daytime Cloud Optical and Microphysical Properties Algorithm (DCOMP) in PATMOS-x. *J. Appl. Meteor. Climatol.*, **51**, 1371–1390, doi:10.1175/JAMC-D-11-0108.1.

——, W. Straka, and A. K. Heidinger, 2011: ABI algorithm theoretical basis Document for Daytime Cloud Optical and Microphysical Properties (DCOMP). NOAA/NESDIS/STAR Algorithm Theoretical Basis Doc., 61 pp. [Available at http://www.goes-r.gov/products/ATBDs/baseline/Cloud_DCOMP_v2.0_no_color.pdf.]

Wilks, D. S., 1995: *Statistical Methods in the Atmospheric Sciences: An Introduction*. International Geophysics Series, Vol. 59, Elsevier, 467 pp.

Xu, X., K. Howard, and J. Zhang, 2008: An automated radar technique for the identification of tropical precipitation. *J. Hydrometeor.*, **9**, 885–902, doi:10.1175/2007JHM954.1.

Zhang, J., C. Langston, and K. Howard, 2008: Brightband identification based on vertical profiles of reflectivity from the WSR-88D. *J. Atmos. Oceanic Technol.*, **25**, 1859–1872, doi:10.1175/2008JTECHA1039.1.

——, and Coauthors, 2011: National Mosaic and Multi-Sensor QPE (NMQ) system: Description, results, and future plans. *Bull. Amer. Meteor. Soc.*, **92**, 1321–1338, doi:10.1175/2011BAMS-D-11-00047.1.

——, Y. Qi, K. Howard, C. Langston, and B. Kaney, 2012: Radar Quality Index (RQI)—A combined measure of beam blockage and VPR effects in a national network. *IAHS Publ.*, **351**, 388–393.

——, and Coauthors, 2016: Multi-Radar Multi-Sensor (MRMS) quantitative precipitation estimations: Initial operating capabilities. *Bull. Amer. Meteor. Soc.*, **97**, 621–638, doi:10.1175/BAMS-D-14-00174.1.

Brought to you by NOAA Central Library | Unauthenticated | Downloaded 09/22/21 07:18 PM UTC